LLNL-JRNL-413702

LAWRENCE
LIVERMORE
NATIONAL
LABORATORY

Rayleigh-Taylor stabilization by material strength at Mbar pressures

H-S. Park, K. T. Lorenz, R. M. Cavallo, S. M. Pollaine, S. T. Prisbrey, B. A. Remington, R. E. Rudd, R. C. Becker, J. V. Bernier

June 8, 2009

Physics Review Letters

Disclaimer

Rayleigh-Taylor stabilization by material strength at Mbar pressures

Hye-Sook Park, K. T. Lorenz, R. M. Cavallo, S. M. Pollaine, S. T. Prisbrey, B. A. Remington, R. E. Rudd, R. C. Becker, and J. V. Bernier

Lawrence Livermore National Laboratory
Livermore, CA, USA

Abstract

Studies of solid-state material dynamics at high pressures (~1 Mbar) and ultrahigh strain rates (>10^6 s^{-1}) are performed using a unique laser based, quasi-isentropic high-pressure acceleration platform. Vanadium foils with pre-imposed sinusoidal ripples are accelerated in the solid state with this ramped high pressure drive. This causes Rayleigh-Taylor (RT) instability growth at the interface, where the rate of growth is sensitive to the solid-state material properties. The RT growth history is measured by face-on radiography using synchronized laser-driven x-ray backlighters at the Omega Laser. The experimental results are compared with 2D hydrodynamics simulations utilizing constitutive models of high pressure material strength. We find that the vanadium strength increases by a factor of 3.5-4 at peak pressure, compared to its ambient (undriven) strength. Both pressure hardening and strain rate hardening are the suggested cause for this increase in strength. An analysis treating strength as an effective lattice viscosity finds that a viscosity of ~400 poise is required to reproduce our RT data.

The Rayleigh-Taylor (RT) instability is of considerable interest to a diverse range of fields. Examples include inertial confinement fusion (ICF) capsule implosions, [Lindl 1995; Betti 1995; Takabe 1985] supernova explosion dynamics, [Muller, 1991; Kifonidis 2006], asteroid and meteor impact dynamics, [MacLow, 1994; Shuvalov, 2002] and heavy ion nuclear multi-fragmentation, [Moretto, 1992] to name just a few. In ICF, a key aspect is the phenomena of ablative stabilization of the RT instability, which plays a critical role in damping the rate of growth of the shortest wavelength modes. In simulation studies of meteor or asteroid impacts, RT instability plays a key role in determining whether the object fragments in the atmosphere, and the size distribution of the fragments.

In the reference frame of the asteroid entering the atmosphere, the high velocity inflowing atmosphere stagnates on the asteroid leading to a net force of acceleration. This triggers the RT instability, which is moderated or stabilized by the material strength or effective viscosity of the asteroid. Experimental data in this unique regime of material strength stabilized RT instability growth is rare, due to the difficult requirements of (1) sufficiently intense drive (acceleration) to force RT instability growth in a solid, but (2) sufficiently "gentle" ramped drive so as to not melt the solid. We report here results of a unique experiment using a laser generated ramped drive. Our experiment follows a scenario similar to the asteroid entering the atmosphere, only we accelerate the "atmosphere" into an initially static sample.

We use the Omega Laser to drive a strong shock (~ 5-10 Mbar) through a sacrificial plastic reservoir, which unloads across a vacuum gap, accelerating this plasma "atmosphere" into the initially static sample, as illustrated schematically in Fig. 1. When the unloading reservoir stagnates on the sample, this generates a nearly isentropic ramped, ~1 Mbar pressure profile on the 35 μm thick vanadium sample, which reaches a peak acceleration of ~0.5 $\mu m/ns^2$ (5×10^{13} cm/s^2). Vanadium is a BCC ductile metal and it is expected to have a significant strain rate dependence in its strength behavior. Its relatively low density (6.1 g/cm^3) means the sample can be easily accelerated at Omega, and has a low enough optical depth for the use of conventional x-ray radiography techniques. We use 6 azimuthally symmetric laser beams each with ~135 J at laser wavelength of λ_L=351 nm and 3.7 ns square pulse shape. The smooth ~640 μm diameter super-Gaussian spatial profile is achieved using distributed phase plates on the drive beams, [Lin, 1995] creating an average peak laser intensity of $I_L \sim 2.5 \times 10^{13}$ W/cm^2. When these drive lasers are focused onto the 40 μm-thick polyimide ablator, they launch a strong shock (5-10 Mbar) into reservoir made of 125 μm thick polycarbonate and 35 μm thick 2% brominated polystyrene, $C_{50}H_{48}Br_2$. This CH(Br) layer absorbs low energy x-rays generated by the direct laser ablation process. When the shock breaks out the back side of the reservoir, the shocked plasma releases (unloads) across the 300 μm vacuum gap and stagnates on the sample, creating the ramped pressure drive. [Edwards 2004; Lorenz 2006] In order to insulate the rippled vanadium sample from the heat created by the initial stagnating plasma, we use a 6 μm thick epoxy layer, conformal on the ripple side and machined flat on the gap side, as a heat shield.

We measure the drive profile using a VISAR [Celliers, 1998] on separate drive targets consisting of a 10 μm thick Al witness plate backed by a LiF window. A raw VISAR image from one of our drive shots is shown in the inset of Fig. 2a. The particle velocity of the back surface of the Al sample was measured by VISAR for a range of laser energies (E_L), as shown by the curves in Fig. 2a. Analysis of these data shows that the peak particle velocity and the initial loading time scale with E_L according to $V_{peak} \sim E_L^{0.768}$ and $t_{loading} \sim 1/E_L^{0.768}$, respectively. We then use the radiation-hydrodynamics code LASNEX [Zimmerman, 1975] to generate a plasma drive, namely, the plasma density, velocity, and temperature vs. position just prior to stagnation on the sample, scaled to the exact E_L of the V-RT shots. This stagnating plasma drive generates the 900 kbar ramped pressure drive that accelerates the rippled vanadium RT sample, as shown in Fig. 2b. The sample is predicted to stay factors of 3-5 below the melt temperature, as shown by the simulated melt and sample temperature profiles (see the inset of Fig. 2b).

The RT target is made by sputtering vanadium onto an Al coated Cu mandrel that has sinusoidal ripples with 60 μm wavelength and 0.6 μm amplitude (peak-to-valley perturbation height of 1.2 μm) diamond-turned onto its surface. The mandrel is chemically etched away and the back surface is polished to achieve a 35 μm average vanadium thickness. The vanadium samples were full density, had an average grain size of ~ 1 μm in the lateral direction and 3-5 μm in the thickness (columnar) direction, and a measured tensile strength (at ambient pressure and low strain rate) of 715 MPa [Jankowski, 2007].

To measure the RT ripple growth, we used face-on radiography with a 5.2 keV laser driven vanadium He-α x-ray backlighter, either in an area backlighting or a point projection imaging configuration. The area backlighting technique used a large area x-ray source and a gated x-ray pinhole camera at magnification of ~6, as described elsewhere. [Lorenz, 2005] The point projection technique used a ~15 μm diameter pinhole aperture just in front of the V backlighter foil to create a point x-ray source for projection imaging at magnification of ~19, also onto a gated x-ray microchannel plate (MCP), with a gate duration of ~200 ps. Figure 3 (right hand side) shows examples of radiographic images of ripple growth at delay times of 40ns and 80 ns relative to the start of the drive laser. Lineouts of the ripples averaged over a 120 μm vertical window are plotted in Fig. 3 (left hand side), compared with fits using $\ln(I_v/I) = a \cdot \sin(\frac{2\pi}{\lambda} - \phi)$. Here I is the measured average intensity through the rippled foil, I_v is the measured intensities in the valleys (brighter regions), and the fit parameters a, λ, and ϕ are the amplitude, period and the phase of the ripple. The ripple growth is written as a growth factor, $GF(t) = \frac{\Delta OD(t)}{\Delta OD_0 \ MTF} f(E_L)$, where $\Delta OD(t)$ is the optical depth modulation due to the ripple at time t, $\Delta OD_0 = \eta_0/\lambda_{mfp}$ is the initial optical depth (η_0 is the initial ripple amplitude of 0.6 μm and λ_{mfp}~19.6 μm is the mean free path of the 5.2 keV backlighter x rays in vanadium), MTF is the modulation transfer function, and $f(E_L)$ is a small laser energy correction factor. The $\Delta OD(t)$ is measured from the radiograph by a Fourier analysis of the ripple lineouts, which is equivalent to the amplitude of a sinusoid fit to the data, as described in Fig. 3. The MTF is measured on a separate shot using a resolution grid. The resulting MTF is given by $M(k) = e^{-(k\sigma)^2/2}$, where k = 2π/λ, (λ being the period of a sinusoid), and σ is the Gaussian point spread function standard deviation. Most of our data had MTF > 80% for the 60 μm wavelength modulations. The laser energy correction factor, $f(E_L)$, accounts for the fact that each shot had a slightly different laser energy (differing by ~10%). We analyzed a set of images from four separate laser shots that were taken at the same delay times. Their corresponding GF without the $f(E_L)$ correction gave a linear relation between the GF and laser energy, E_L. We then normalized all measured

GFs to a standard average laser energy of 819 J, producing a single, self-consistent data set, as shown by the square symbols in Fig 4. The errors include the fitting, statistical, and systematic errors. Typical errors were δGF/GF ~10% or less. We estimate the average strain rate by fitting a linear slope to the calculated strain at early, intermediate, and late times. The resulting strain rates ranged from 3 x 10^7 s^{-1}, at early times near peak pressure (25-30 ns), and 3 x 10^6 s^{-1} later in time, at t > 40 ns (see Fig. 2b).

We compare in Fig. 4 our RT growth factor measurements to the results from 2D radiation-hydrodynamics simulations, including constitutive strength models, concentrating on two strength models: the Stenberg-Guinan (SG) model [Steinberg, 1980] and the Preston-Tonks-Wallace (PTW) model. [Preston, 2003] The SG model assumes that the strength is given by the initial strength times factors due to work (strain, ε) hardening and pressure hardening, namely, $\sigma_{SG}=\sigma_0 f(\varepsilon)G/G_0$, where σ_0 and G_0 are the ambient strength and shear modulus, and $f(\varepsilon)=[1+\beta(1+\varepsilon)]^n$ is the work hardening factor, where β and n are the work-hardening parameters. The shear modulus, $G=G(P,T,G_P',G_T')$ is a function of pressure (P), temperature (T), and the partial derivatives of G with P and T. Hence, G/G_0 represents the pressure hardening factor. Note, in the SG model, there is no explicit dependence on strain rate.

The PTW model is strain rate dependent, and is based on the deformation mechanisms of thermal activation for low strain rates and viscous phonon drag for high strain rates. [Preston, 2003] The dimensionless shear strength in the low-strain limit is expressed as:

$$\hat{\tau}_y = \max\left\{ y_0 - (y_0 - y_\infty) erf[\kappa \hat{T} \ln(\gamma \dot{\xi} / \dot{\varepsilon})], s_0 (\dot{\varepsilon} / \gamma \dot{\xi})^\beta \right\} \tag{1}$$

where, $\dot{\varepsilon}$ is the strain rate, $\hat{T}$ is the normalized temperature, $\dot{\xi}$ is an reference inverse time scale, and y_0, y_∞, κ, γ, s_0, and β are material dependent input parameters. The dimensionless shear strength, $\hat{\tau}_s$, in the high-strain limit has a similar form, only replacing y_0 and y_∞ with s_0 and s_∞. These are combined in a Voce work hardening prescription to give the predicted (dimensional) material strength as:

$$\sigma_{PTW} = 2G(P,T)\left\{\hat{\tau}_s - (\hat{\tau}_s - \hat{\tau}_y)\exp\left[-\left(\frac{\theta\varepsilon}{\hat{\tau}_s - \hat{\tau}_y}\right)\right]\right\} \tag{2}$$

In Fig 4, the top curve corresponds to a 2D simulation of the RT growth assuming no strength in the material. Note, the predicted growth factors without strength at 70 ns are large, GF ~ 70, which is a factor or ~6 higher than the experimental data. Simulations using the SG and the PTW models with the default input parameters for vanadium [Steinberg, 1980; Preston, 2003] are the next two highest curves in Fig. 4, and both also considerably over-predict the experimental data. Since the nominal input parameters of these models were derived mainly from low pressure data, this disagreement is not surprising. To match the experiment, we increased σ_0 in the S-G model by a factor of 1.9 above the measured ambient strength [Jankowski, 2007]; the result is shown by the solid green solid curve in Fig 4. The interpretation of this is not that the ambient strength, σ_0, was higher than measured, but rather that the S-G model is missing the significant effect of strain rate hardening.

To fit our experimental data with the PTW model, we chose to lower the critical strain rate for the transition from thermal activation to the phonon drag regime. This was accomplished by multiplying the PTW input parameters γ, y_0, and s_0 by 1/7000, 0.27, and 0.41, respectively. This leaves the PTW strength predictions at $d\varepsilon/dt < 10^6$ s^{-1} largely unchanged, while increasing the strength for $d\varepsilon/dt > 10^6$ s^{-1}. Analysis of the PTW equations suggests that the input parameter γ corresponds to dislocation density, ρ_{disloc}, namely, $\gamma \sim \rho_{disloc}b^2$, where b is the Burgers vector. [Remington, 2006] We interpret the large reduction in γ as resulting from the significantly lower ρ_{disloc} from a ramped compression, compared to the strong shock data for which PTW was originally calibrated at the highest strain rates. [Bringa, 2006] The simulation result is shown as the solid blue curve in Fig. 4. The calculated peak flow stresses for both models for our RT experiments are shown in the inset of Fig. 4. The average of all these points is 25.8±0.6 kbar, which we take as our inferred peak strength corresponding to a peak pressure and strain rate of 900 kbar and 3 x 10^7 s^{-1}. This is a factor of 3.6 higher than the ambient value of 7.15 kbar, confirming that vanadium strength increases significantly at high - (P, $\dot{\varepsilon}$). These two models, when fit to the same RT data, give similar peak flow stress to within ~5%, suggesting that this RT approach for inferring high-(P,dε/dt) strength is not particularly model dependent.

We also give an analysis treating the strength as an effective lattice viscosity. In the classical, linear regime, the RT growth factor can be written as $GF \approx e^{\int \gamma_{classical} dt}$, where $\gamma_{classical} \approx [A \cdot \frac{2\pi}{\lambda} \cdot g(t)]^{1/2}$ gives the growth rate for inviscid fluids, A, λ, and g are the Atwood number, perturbation wavelength, and foil acceleration, resp. For viscous fluids, the RT growth rate is expressed in the dispersion relation, $\gamma_{vis}^2 + 2k^2 \nu \gamma_{vis} - gkA = 0$, [Mikaelian, 1993; Colvin, 2003], where $\nu(cm^2/s) = \mu/\rho$ is the kinematic viscosity, μ(dyne·sec/cm^2=Poise) is the dynamic viscosity, and ρ is density. We show these analytic results in Fig. 5 compared to RT growth factors at 70 ns versus perturbation wavelength. Experimental data were taken only at λ = 40 μm and 60 μm (red plotting symbols). The 2D simulations were done at λ = 40, 60, and 100 μm with the modified strength models (brown plotting symbols), and with strength turned off (black plotting symbols). The analytic classical inviscid RT calculation for no strength is shown by the blue curve. The four lower curves (green, brown, purple) are for the classical viscous fluid model, with dynamic viscosities of 300, 400, and 500 Poise. The best fit viscosity was ~400 poise. We also shown in Fig. 4 (solid orange curve) the time evolution, GF(t), for the viscous model using 400 poise. As a consistency check, we use a relationship equating strength with an effective lattice viscosity, $\nu = \mu / \rho \approx \sigma / (\sqrt{6} \rho \dot{\varepsilon})$, [Colvin, 2003] giving $\sigma \approx \sqrt{6} \dot{\varepsilon} \mu$. Using the peak average strain rate of 3 x 10^7 s^{-1} and the fitted viscosity of 400 poise gives an estimated peak strength of 29 kbar, compared to that inferred from the 2D simulations of 26 kbar, which is quite reasonable agreement.

In conclusion, we have developed an experimental platform that allows solid-state samples to be compressed quasi-isentropically in a high-pressure ramp wave, maintaining the sample factors of several below their melt temperature. The strain rates are very high, $\langle d\varepsilon/dt \rangle = 3 \times 10^6 - 3 \times 10^7\ s^{-1}$, due to the applied ramped pressure, with $P_{max} \sim 900$ kbar. The RT instability growth is reduced (stabilized) by material strength. Within the framework of the PTW strength model, the mechanism of deformation is inferred to be viscous phonon drag. In an effective lattice viscosity treatment, a viscosity of ~400 poise is required to reproduce the experimental data.

Acknowledgement: This work was performed under the auspices of the U. S. Dept. of Energy by Lawrence Livermore National Laboratory under Contract No. DE-AC52-07NA27344.

References:

[Betti 1995] R. Betti et al., Phys. Plasmas 2, 3844 (1995).

[Bringa, 2006] E. Bringa et al., Nat. Mat. 5, 805 (2006).

[Celliers, 1998] P.M. Celliers et al., Appl. Phys. Lett. 73, 1320 (1998).

[Colvin, 2003] J.D. Colvin et al., J.Appl.Phys. 93, 5287 (2003).

[Edwards, 2004] J. Edwards et al., PRL 92 (2004), 075002.

[Jankowski, 2007] A.F. Jankowski, J. Go, and J.P. Hayes, Surface & Coatings Tech. 202 (2007), 957.

[Kifonidis 2006] K. Kifonidis et al., Astron. Astrophys. 453, 661 (2006).

[Lin, 1995] Y. Lin, T.J. Kessler, and G.N. Lawrence, Optics Lett. 20, 764 (1995).

[Lindl 1995] J.D. Lindl, Phys. Plasmas 2, 3933 (1995).

[Lorenz, 2005] K.T. Lorenz et al. Phys. Plasmas 12 (2005), 056309.

[Lorenz, 2006] K.T. Lorenz et al. HEDP 2 (2006), 113.

[MacLow, 1994] Mordecai-Mark MacLow and Kevin Zahnle, Ap.J.Lett. 434, L33 (1994).

[Mikaelian, 1993] Karnig O. Mikaelian, Phys. Rev. E 47, 375 (1993).

[Moretto, 1992] L.G. Moretto et al., Phys. Rev. Lett. 69, 1884 (1992).

[Muller, 1991] E. Muller et al., Astron. Astrophys. 251, 505 (1991).

[Park, 2008] H. S. Park et al., J. Phys.: Conf. Ser. 112, 042024 (2008).

[Preston, 2003] D.L. Preston, D.L. Tonks, and D.C. Wallace, J. Appl. Phys. 93, 211 (2003).

[Remington, 2006] B.A. Remington et al., Mat. Sci. Tech. 22, 474 (2006).
[Steinberg, 1980] D.J. Steinberg, S.G. Cochran, and M.W. Guinan, J. Appl. Phys. 51, 1498 (1980).
[Shuvalov, 2002] V.V. Shuvalov et al., Planetary and Space Science 50, 181 (2002).
[Takabe 1985] H. Takabe et al., Phys. Fluids 28, 3676 (1985).
[Zimmerman, 1975] G.B. Zimmerman and W.L. Kruer, Com. Plasma Phys. Control. Fusion 2, 51 (1975).

Figure Captions:

Fig. 1 Schematic illustrating the experimental configuration. Drive lasers shock a plastic reservoir, which releases across a vacuum gap as a flowing plasma atmosphere. This generates a ramped pressure drive, upon stagnation on the vanadium (V) sample. A second set of lasers, delayed in time, drives an x-ray backlighter for face-on radiography of the Rayleigh-Taylor instability growth in the rippled V sample.

Fig. 2 Drive characterization measurements. (a) VISAR drive measurements for four different laser energies spanning 750 – 850 J, for a configuration similar to that shown in Fig. 1, except that the sample was 10 μm Al backed by a ~500 μm thick LiF window. (b) Corresponding pressure vs. time in the vanadium RT sample, as calculated from 1D radiation-hydrodynamics simulations, adjusted to reproduce the drive measured in the Al-LiF witness plates shown in (a). The inset shows the melt temperature and sample temperature from the 1D simulation.

Fig. 3 Raw 2D x-ray radiographs of driven V-RT samples at 40 ns (lower RHS) and 80 ns (upper RHS). Corresponding lineouts vertically averaged over 120 μm of Log(Intensity) on the LHS at the same two times.

Fig. 4 Measured and simulated RT growth factors vs. time. The solid square plotting symbols give the experimental data, as described in the text. The top curve (orange dot-dashed) gives the result from the simulation with strength set to zero. At t = 70 ns, this no-strength simulation gives growth factor (GF) of 67. The next highest curve (green dotted) gives the results of the 2D simulation using the Steinberg-Guinan (SG) strength model, using the default input parameters for vanadium. Below that, the blue dot-dashed curve gives the simulation result using the PTW model with default input parameters. The solid green curve is the result of increasing the measured ambient strength by a factor of 1.9 in the SG model. The solid blue curve corresponds to the PTW model, with the default vanadium input parameters γ, y_0, s_0 multiplied by 1/7000, 0.27, and 0.41. The lower solid orange curve corresponds to an analytic approach treating the material strength as an effective lattice viscosity, in this case with a value of 400 poise. The inset gives peak strength for the SG and PTW models for all of the experiments done in the V-RT campaign. Note that the experiments covered a range of drive laser energies, corresponding to peak pressures in the V sample of 760 - 930 kbar.

Fig. 5 Measured, simulated, and theoretical RT dispersion curves, given as growth factor vs. perturbation wavelength at a time of 70 ns. The solid circle plotting symbols correspond to a 2D radiation-hydrodynamics simulation with material strength set to zero; the blue diamond solid plotting symbols to a 2D radiation-hydrodynamics simulation with the PTW strength model adjusted to fit the experiment; the green triangle solid plotting symbols to a 2D radiation-hydrodynamics simulation with the Steinberg-Guinan (SG) strength model adjusted to fit the experiment. The square red plotting symbols correspond to the experimental measurements.

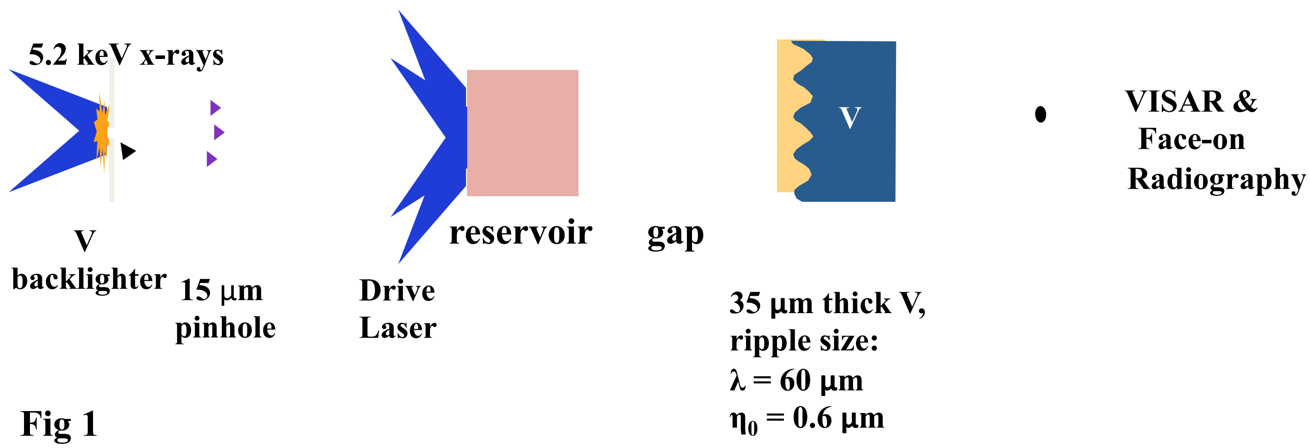
5.2 keV x-rays
V
backlighter
15 μm
pinhole
Drive
Laser
reservoir
gap
V
35 μm thick V,
ripple size:
λ = 60 μm
η0 = 0.6 μm
VISAR &
Face-on
Radiography

Fig 1

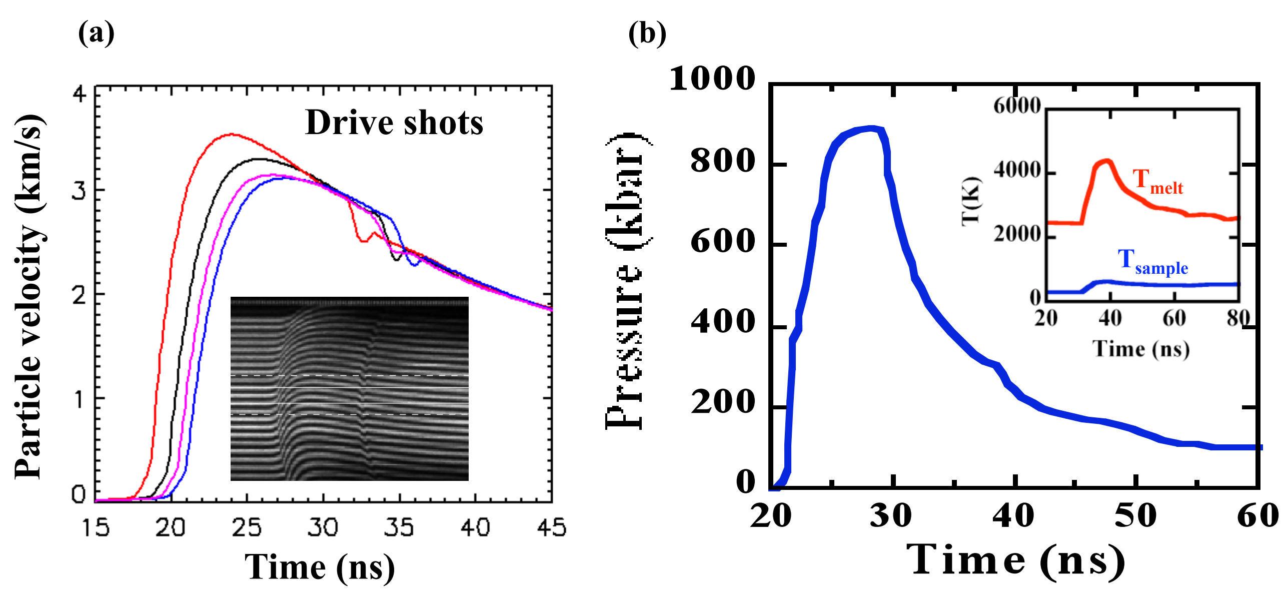
(a)
Drive shots
Particle velocity (km/s)
Time (ns)
(b)
Pressure (kbar)
Time (ns)
T(K)
Tmelt
Tsample
Time (ns)

Fig 2

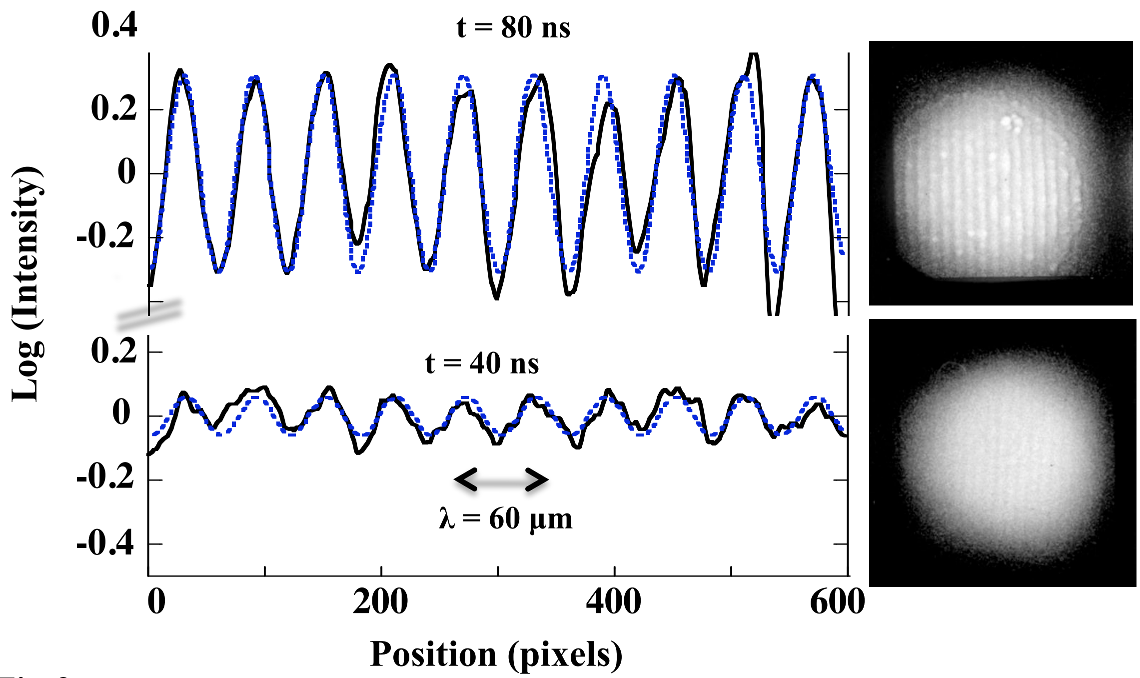
t = 80 ns
t = 40 ns
λ = 60 μm
Log (Intensity)
Position (pixels)
0.4
0.2
0
-0.2
-0.4
200
400
600

Fig 3

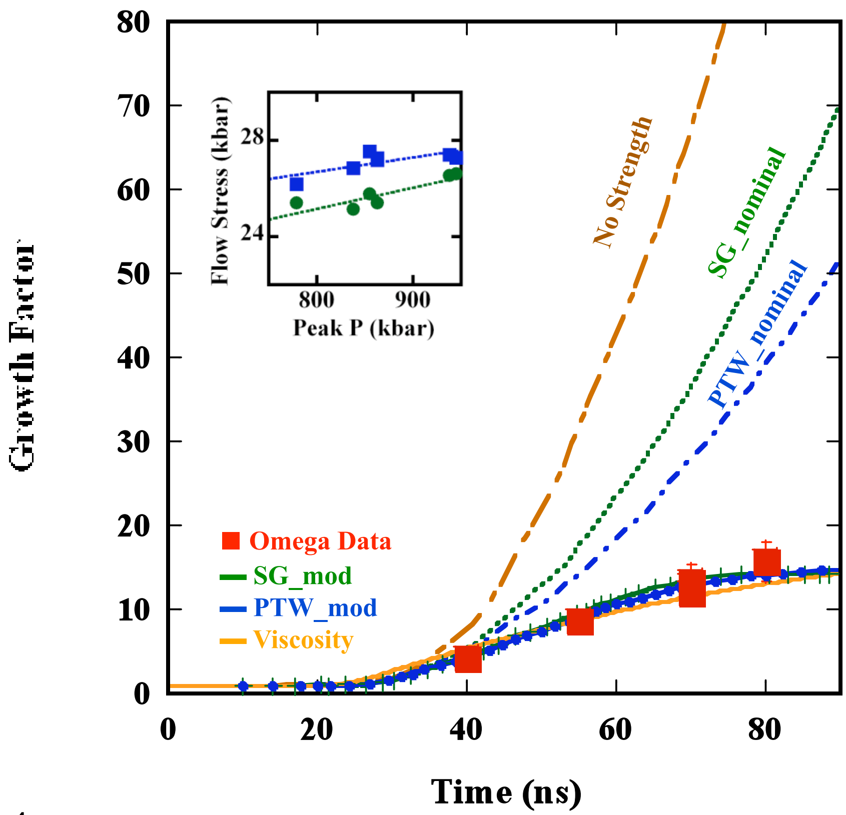
No Strength
SG_nominal
PTW_nominal
Omega Data
SG_mod
PTW_mod
Viscosity
Flow Stress (kbar)
Peak P (kbar)
28
24
800
900
Growth Factor
Time (ns)
80
70
60
50
40
30
20
10
0

Fig 4

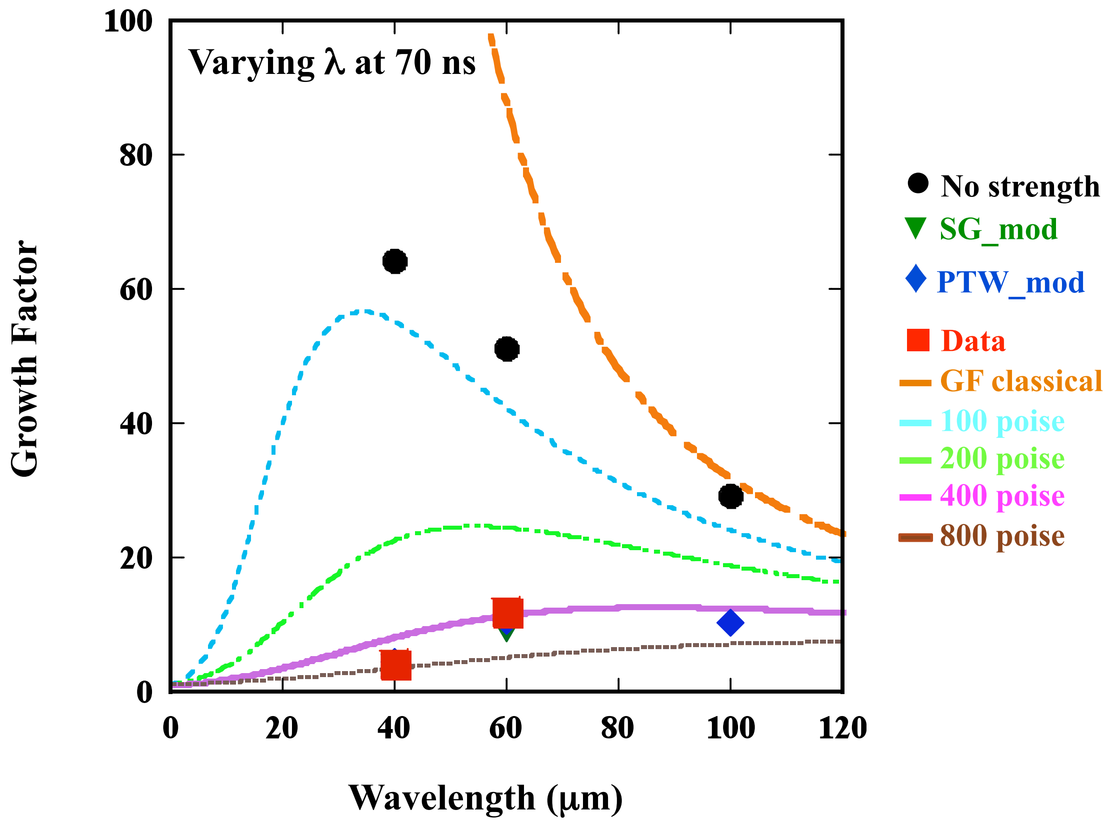
Varying λ at 70 ns
Growth Factor
Wavelength (μm)
0
20
40
60
80
100
120
No strength
SG_mod
PTW_mod
Data
GF classical
100 poise
200 poise
400 poise
800 poise

Fig 5